Type of the Paper (Article)

Optical constants of rare-earth substituted ferrite-type amorphous garnets and nanoscale garnet-oxide layers

Mohammad Nur-E-Alam*, Mikhail Vasiliev and Kamal Alameh

Affiliation: Electron Science Research Institute, School of Science, Edith Cowan University, 270 Joondalup Drive, Joondalup 6027, WA, Australia; m.nur-e-alam@ecu.edu.au (MNA); m.vasiliev@ecu.edu.au (MV); k.alameh@ecu.edu.au (KA).

* Correspondence: m.nur-e-alam@ecu.edu.au

Abstract: Amorphous ferrite-type rare-earth (RE) substituted garnets and garnet-oxide nanocomposite layers are prepared on clear glass substrates by using RF magnetron sputter-deposition process. By using a combination approach employing custom-built spectrum-fitting software in conjunction with Swanepoel's envelope method, the spectral dispersion function of optical constants and the layer thicknesses are derived accurately from the transmission spectra of the as-deposited samples. The effects of excess metal-oxides added to the base material systems during the co-deposition process are found to affect the refractive index and the optical absorption coefficients of garnet-oxide composites. A number of optical constant datasets are presented, enabling the experimentalists to design nanophotonic or integrated-optics devices employing these functional materials.

Keywords: rare-earth garnets; optical constants; envelope method; nano-composites; magneto-optics.

1. Introduction

Rare-earth substituted ferrite garnet-type thin-film materials are in high demand in modern magneto-optics (MO) and nano-scale devices for use in various applications. During the last couple of decades, many researchers and engineers worldwide have conducted a significant amount of work in the field of MO garnet thin film materials. These works have their origins from the days of bubble-domain magnetic disk memory development, when the substitution of rare-earth ions (e.g. Bi^{3+}, Ce^{3+} and others) into the Yittrium Iron garnet (YIG) material system was found to significantly enhance the Faraday rotation properties. The rare-earth ions substitution into the dodecahedral sublattice sites of garnet mainly affects the structural (lattice constant), optical (refractive index and absorption coefficient), and also the magnetic and magneto-optic properties of iron garnet thin film materials. More recently, other non-magnetic (e.g. Ga or Al) ions have been introduced to the ferrite garnet systems, which tend to occupy the octahedral and tetrahedral garnet sublattices, also affecting magnetic and MO properties. A huge variety of rare-earth and other metal dopants have been introduced into different garnet-type systems, and their properties studied extensively to overcome the practical difficulties of using these ferrite-type garnets in various new and existing technologies [1-14], e.g. to increase the specific Faraday rotation simultaneously with reducing the annealing process temperature. The demand for application-specific MO garnets is still growing, since the need for on-chip integration of MO/MPC non-reciprocal photonic devices is rapidly becoming imperative day by day [15-20].

 doi:10.20944/preprints201902.0250.v1

However, the development of high-quality thin-film garnet materials requires a significant amount of characterization and investigation of all material properties of interest. Most of the previous reports of substituted iron-garnet films include optical absorption, Faraday rotation, MO figure of merit, and magnetic hysteresis loop measurement results for either a single wavelength or within a narrow spectral range [7-14, 21-25]. Despite the growing interest in using garnet films, to the best of our knowledge, there are no comprehensive reports on the easy determination of optical constants data of garnet thin films. Moreover, the detailed reports in which the refractive index dispersion functions of MO garnets have been presented, are relatively scarce. Therefore, determination of the optical constants (complex refractive index) by a non-destructive and cost-effective method is an important part of material characterization, which is necessary whenever any new garnet composition is developed. The accurate determination of optical constants data across a wide spectral range for each particular rare-earth-substituted garnet material is crucial for the design and optimization of any MO or MPC-based modern devices operating at different wavelengths e.g. active displays, image sensors, magneto-optic sensors and imagers, and magneto-plasmonic biosensors. Spectroscopic ellipsometry and profilometry are well-known technologies used to determine the physical thickness and/or refractive index of thin-film materials, but these are often very complex, and costly equipment is required. However, based on both the transmission and reflection spectra, several calculation methods have been reported to derive the refractive index (mainly, its real part) and the film thickness [26-31]. All of these methods are applicable (within certain limitations) to determine the refractive index of thin films using the optical interference fringes of the transmission and reflection spectra. Measurement accessories for spectrophotometers capable of measuring the reflection spectra are costlier and less accessible compared to equipment measuring transmission spectra only. In this work, we derive accurately the optical constants data for multiple rare-earth doped iron garnets simultaneously with the garnet film thicknesses from the optical transmission spectra by means of a combinatorial approach of employing custom-built spectrum-fitting software in conjunction with Swanepoel's envelope method [32]. We apply the measurement methodology described in subsequent section to a very broad spectral range between 400 nm to over 2000 nm to generate optical property datasets for multiple MO garnet compositions of interest to future device developers.

2. Theory and equations used to process transmission fringes and derive the refractive index and film thickness data

Swanepoel's envelope method (SWEM) [26-28, 30-32] can be used to calculate an approximate value of the refractive index of semitransparent and weakly-absorbing thin film media. Amorphous garnet-type nanoscale layers grown on clear glass substrates represent an appropriate medium to apply SWEM to determine their optical constants. The basic equation given below can be used to calculate the approximate refractive index values of garnet films by using the spectral locations of the transmission maxima and minima:

$$n_1 = \left[N + (N_2{}_{-}S_2)^{1/2}\right]^{1/2} \quad \text{..(1)}$$

where the value of N can be determined from the following expression: $N = 2S\{(T_M - T_m)/T_M.T_m\} + (S^2+1)/2$; here T_M and T_m denote the maximum and minimum transmittance at a given wavelength, respectively. Parameter S represents the refractive index of used glass substrate (averaged across the spectral range of interest), which is 1.47 for the Corning glass substrates used in this work.

Figure 1 shows an example of typical transmission spectrum of a garnet film presenting the envelopes transmission maxima (T_M) and minima (T_m) intensities.

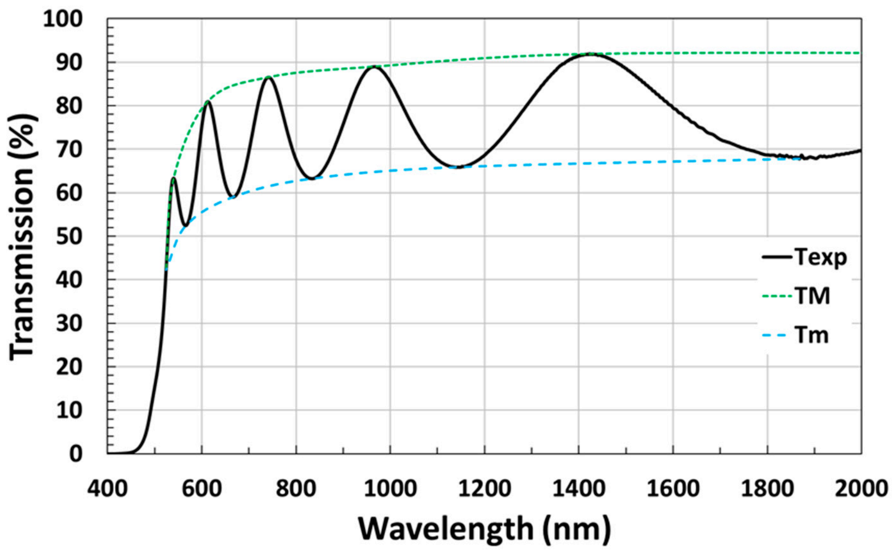

Figure 1. Example of a typical transmission spectrum of a garnet thin film sample of composition type $Bi_{2.1}Dy_{0.9}Fe_{3.9}Ga_{1.1}O_{12}$ (the garnet composition characterized within Ref [33]); where Texp is the measured transmission of the sample, T_M and T_m are the maxima and minima of the envelopes.

Using the primary refractive index (approximate n_1, derived from equation 1 at all wavelengths of interest) values into the basic equation of the interference fringes, $2nd = m_0\lambda$, the order number (m_0, which is an integer for maxima and a half-integer for minima) of interference fringes, and the first-approximation value of the film thickness (d_1, as shown in Table 1) can be determined by using the expression:

$$d_1 = \frac{\lambda_1\lambda_{21}}{2(n_2\lambda_1 - n_1\lambda_2)} \qquad (2)$$

where, n_1, and n_2, are the refractive indices at two adjacent maxima (or minima) at λ_1 and λ_2.

Table 1: Example of calculated results for a typical garnet thin film material deposited on a glass substrate (transmission spectrum is shown in Fig. 1).

1	2	3	4	5	6	7	8	9	10
Sample	**Wavelength (nm)**	**T_M**	**T_m**	**$n_1 = [N + (N^2 - S^2)^{1/2}]^{1/2}$**	**$d_1 = \lambda_1\lambda_2/2(n_2\lambda_1 - n_1\lambda_2)$ (nm)**	**$m_0 = 2n_1d/\lambda$**	**M**	**$d_2 = M\lambda/2n_1$ (nm)**	**$n_2 = M\lambda/2d_{2\,(ave)}$**
A typical garnet type thin film	1868	0.92	0.6779	2.239	-	1.5	1.5	626	2.226
	1430	0.9187	0.6675	2.269	627	2.0	2.0	630	2.272
	1140	0.9056	0.6585	2.276	641	2.5	2.5	626	2.264
	966	0.8895	0.647	2.286	638	3.0	3.0	634	2.302
	834	0.88	0.6323	2.318	630	3.5	3.5	630	2.319
	740	0.8650	0.619	2.338	589	4.0	4.0	633	2.351
	666	0.85	0.5899	2.417	585	4.5	4.5	620	2.381
	612	0.8090	0.56	2.457	671	5.0	5.0	623	2.431
	566	0.745	0.5244	2.475	781	5.5	5.5	629	2.473
	540	0.6333	0.46	2.513	-	-	-	-	-

d_1 (ave) = 626 nm, δ_1 = 24.8 nm (3.96%), d_2 (ave) = 629 nm, δ_2 = 4.82 nm (0.76%), $d_{(mpcmf)}$ =630 nm

Preprints (www.preprints.org) | NOT PEER-REVIEWED | Posted: 27 February 2019 doi:10.20944/preprints201902.0250.v1

The detailed explanations of relevant theory are available from Refs [26-28, 32]. The same Refs. Also discuss the reasons for having some inaccuracies in the refractive index and the first-approximation film thickness calculations, and also the ways of reducing the deviations obtained in first-approximation film thickness calculations to obtain an acceptable film thickness values (with a smaller numerical dispersion). After examination of the calculated n and d values, a simple complementary graphical method can be applied to derive the first-order number m_1 and the film thickness d, by modifying the interference fringe expression ($2nd = m_0\lambda$) as given below, for the successive maxima and minima, starting from the long-wavelength end:

$$l/2 = 2d\,(n/\lambda) - m_1 \quad (3)$$

where m_1 is the first-order value, which equals an integer for a maximum and a half-integer for a minimum, and l = 0, 1, 2, 3, …. Therefore, by plotting (l/2) versus (n/λ) (as shown in Fig. 2(a)), a straight line with slope value 2d and cut-off on the Y -axis at (- m_1), the more precise physical thickness d of each thin film sample can be obtained using parameter d_2 ($d = d_2 = 0.5$ x slope value).

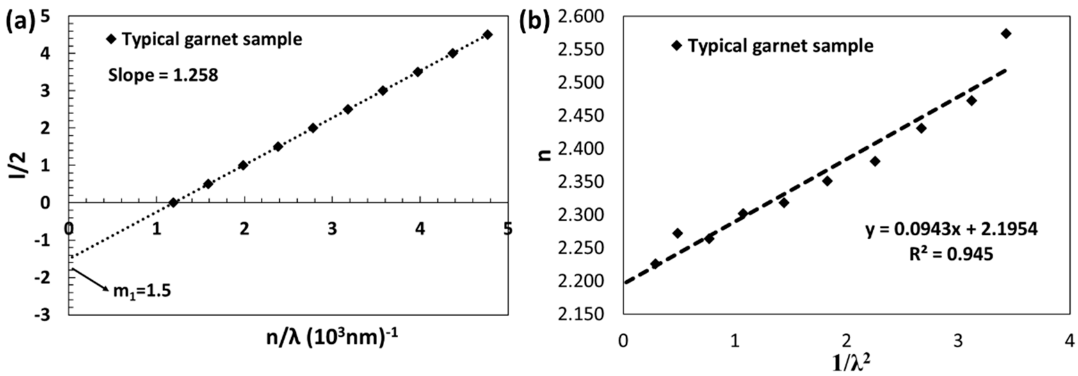

Figure 2. Plots of (l/2) versus (n/λ) (a), and n vs λ^{-2} (b) used to determine the physical film thickness and the first-order value m_1, and also the Cauchy's constants, respectively.

It is also reported that the Cauchy's dispersion formula can be used to derive the values of refractive index over the spectral range between 300-2500 nm, if only the Cauchy's constants are known [27, 28, 30, 32]. By using the calculated values of the final refractive index (from envelope method), in conjunction with least-square fitting (Fig. 2b), the refractive index dataset can be derived using the following expression:

$$n(\lambda) = a + b/\lambda^2 \quad (4)$$

where a and b are Cauchy's constants, which can be determined from the intercept and slope of the n-versus-λ^{-2} linear plot, respectively.

In our previous work, we demonstrated the computational spectral fitting method of film thickness and absorption coefficient derivation using an in-house-built magnetic photonic crystal (MPC) software using the refractive index dispersion data obtained from Cauchy's formula [32].

3. Methodologies and calculation results for the optical constants of several garnet and garnet-oxide composite thin films

In this work, we have carried out the following steps to investigate and determine the film thicknesses and the refractive index datasets from their measured transmission spectra only:

Part (1): Calculate the refractive index data and film thickness by using the SWEM method.

 doi:10.20944/preprints201902.0250.v1

Step (1). The spectral position of the transmission maximum and minimum peaks were determined in the transmission spectrum and listed as shown in the columns 2, 3 and 4 in Table 1.
Step (2). Calculate the approximate values of refractive index and the primary film thickness estimates using the values of transmission maxima and minima and listed (column 5 and 6).
Step (3). The estimated interference fringes order numbers were determined by substituting n_1 values in equation (2), as shown in column 7. Later, the refined interference fringes order numbers (either integer or half-integer) were identified, as listed in column 8.
Step (4). Recalculate the film thickness using the correct interference fringe numbers and listed the film thickness values (with less deviation) in column 9.
Step (5). The final refractive index of the film was recalculated by substituting the correct interference fringe number and the film thickness values in equation 2 as listed in column 10.

Part (2). By using a simple graphical method based on the modified interference fringes equation, the physical film thicknesses were determined and re-checked. The acceptable film thickness (with better accuracy) was found.

Part (3). By using the calculated values of the final refractive index (from envelope method), in conjunction with least-square fitting (derived from n vs λ^{-2} plot), the real parts of refractive index of the films were derived, at each wavelength, using Cauchy's dispersion formula $n(\lambda) = a + b/\lambda^2$, where a, b are the Cauchy's constants.

Part (4). Using the refractive index (derived from Cauchy's dispersion formula) data in MPC spectrum-fitting software, we fitted the transmission spectra with the modeled transmission spectra and re-calculated the film thicknesses. From this fitting process, we then derived the absorption coefficient spectra for all samples using the MPC software, which relied on sufficiently accurate data for both the physical thickness, refractive index dispersion function, and the measured transmission spectrum.

3.1. Optical study of $Y_3Fe_5O_{12}$ and $Y_3Fe_5O_{12}$:Bi_2O_3 (10-30 vol.%) composites

$Y_3Fe_5O_{12}$ (YIG) is one of the most widely known ferrimagnetic garnet crystals among all rare-earth iron garnets that are used in various microwave-range and optical devices such as circulators, isolators, filters, and switches [8, 9, 25]. YIGs do not possess giant Faraday rotation properties in the visible and near-infrared ranges. Various Bi-substituted YIG-derived garnet compositions can possess giant specific Faraday rotations and large MO figures of merit in the visible range, together with narrow ferromagnetic resonance (FMR) linewidths (at about 6.1 Oe at 9.77 GHz[25]) in sputtered nanocomposite-type films with bismuth oxide dilution, which is of significant interest for various modern microwave-range applications and advanced technologies. The methods of synthesis and the measured characteristics for a range of optimized YIG-bismuth oxide ($Y_3Fe_5O_{12}$-Bi_2O_3) composites have been described in detail within the Ref [25]. In this subsection, we present the results of the optical constants study of as-deposited (amorphous) YIG and YIG :Bi_2O_3 (10-30 vol. % of excess oxide) composite nano-scale layers.

Figure 3 shows the measured transmission spectra of as-deposited YIG and YIG : Bi_2O_3 composite garnet layers. All samples showed an adequate number of interference fringes to reliably calculate the film thicknesses and their refractive index data using these transmission fringes. It is well known that thicker films show more fringes of transmission [34]. It can be noticed that the addition of Bi_2O_3 content from a separate metal-oxide target during the co-sputtering deposition process helps shift the optical absorption edge in garnet-oxide composite layers towards the shorter wavelengths. Increasing the volumetric content of Bi_2O_3 added into the composite system improves the optical transmittance in the shorter wavelength region.

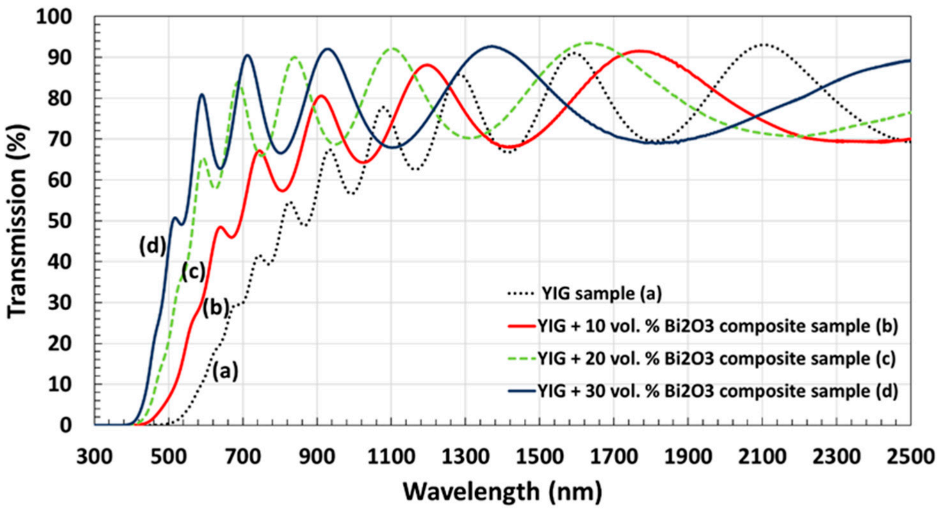

Figure 3. Transmission spectra of as-deposited $Y_3Fe_5O_{12}$ and $Y_3Fe_5O_{12}$:Bi_2O_3 composite thin films deposited on glass substrates. Curve (a) represents a 1434 nm thick $Y_3Fe_5O_{12}$ garnet layer; (b) represents a 811 nm thick $Y_3Fe_5O_{12}$: 10 vol. % Bi_2O_3 composite film; (c) represents a 760 nm thick $Y_3Fe_5O_{12}$: 20 vol. % Bi_2O_3 composite film, and (d) represents a 640 nm thick $Y_3Fe_5O_{12}$: 30 vol. % Bi_2O_3 composite film.

Figure 4 shows the presentation of simple complementary graphical method (l/2 versus n/λ plots) that we applied to derive film thickness with better accuracy (close to 1% deviation). The determination of accurate film thickness is one of the important key factors for reliable calculation of the real part of the refractive index for any type of semi-transparent thin-film materials. The plots (l/2) versus (n/λ) give a straight line of slope equal to twice of the actual film thickness, which intersects the Y axis at ($-m_1$) values for all samples. From this slope value, the actual film thickness can be calculated by following a simple relation, d [nm] = 0.5 × slope value × 1000. The film thickness value for each as-deposited sample was found to be close to the calculated values (calculated using SWEM, as mentioned in the in Table S1 in the Supplementary section).

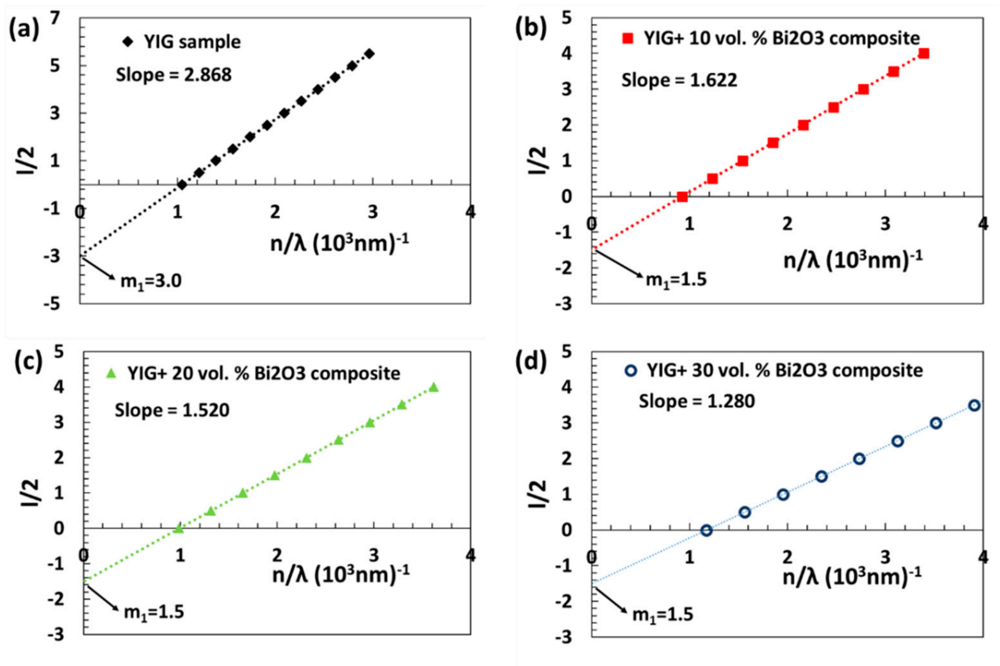

Figure 4. Plots of (l/2) versus (n/λ) used to determine the film thickness and the first-order value m_1 for $Y_3Fe_5O_{12}$ and $Y_3Fe_5O_{12}$:Bi_2O_3 composite thin films. The Y-axis cut-off (m_1) and the slope values for each sample are illustrated in the graphs.

Preprints (www.preprints.org) | NOT PEER-REVIEWED | Posted: 27 February 2019 doi:10.20944/preprints201902.0250.v1

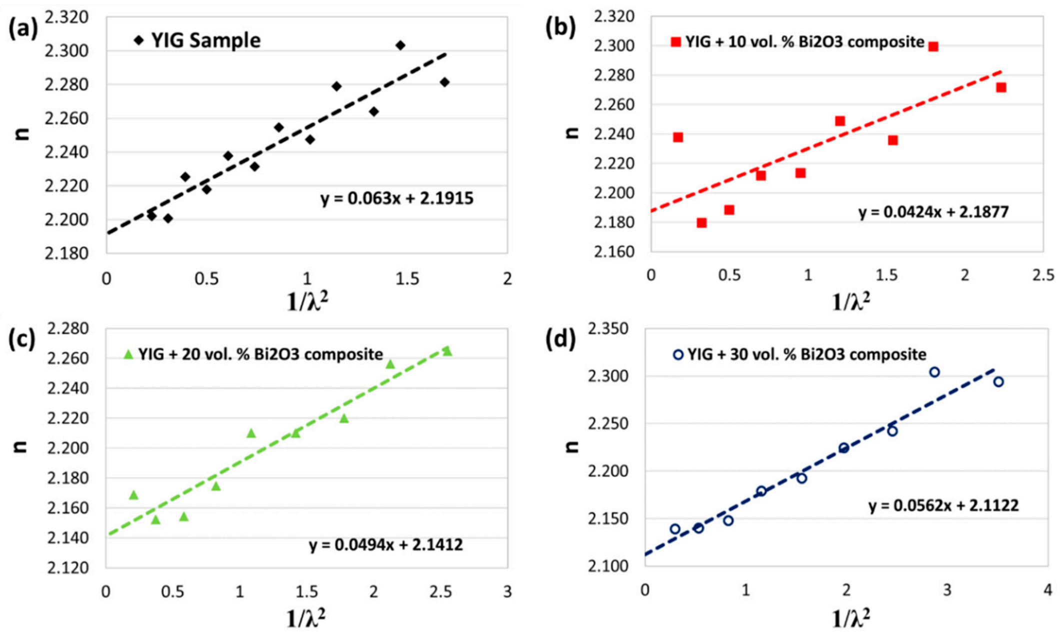

Figure 5. Least-square fits of the calculated refractive index (n_2) values for $Y_3Fe_5O_{12}$ and $Y_3Fe_5O_{12}$:Bi_2O_3 composite-type co-sputtered thin films.

Figure 5 shows linear plots of least-square fits (n vs λ^{-2}), from where the values of Cauchy's constants (a, and b) were determined. By substituting the a and b values into Cauchy's dispersion formula Equation (Eq. 4), the values of the refractive index were derived over the whole spectral range of measurement, between 300–2500 nm, as shown in Figure 6. In Figure 6, the data points of n_2 values are represented as solid large points, while n values derived by using Cauchy's dispersion relation for the corresponding sample are plotted as solid lines. From this figure, one can note that the increasing volumetric fraction of Bi_2O_3 introduced into the YIG material system helps to reduce to refractive index of the films across the spectrum, thus improving the optical transparency. The transparency has also been improved substantially due to obtaining lower absorption coefficients in nanocomposites, compared to the pure YIG sample. It is likely that, in the nanocomposite materials system, an increased substitution of Bi^{3+} ions occurs within the dodechadral sublattice sites of YIG, thus increasing the specific Faraday rotation. At the same time, diluting the highly-absorbing garnet phase and residual iron oxides with a high-transparency oxide material (Bi_2O_3) leads to reduced optical absorption [22, 25].

Preprints (www.preprints.org) | NOT PEER-REVIEWED | Posted: 27 February 2019 doi:10.20944/preprints201902.0250.v1

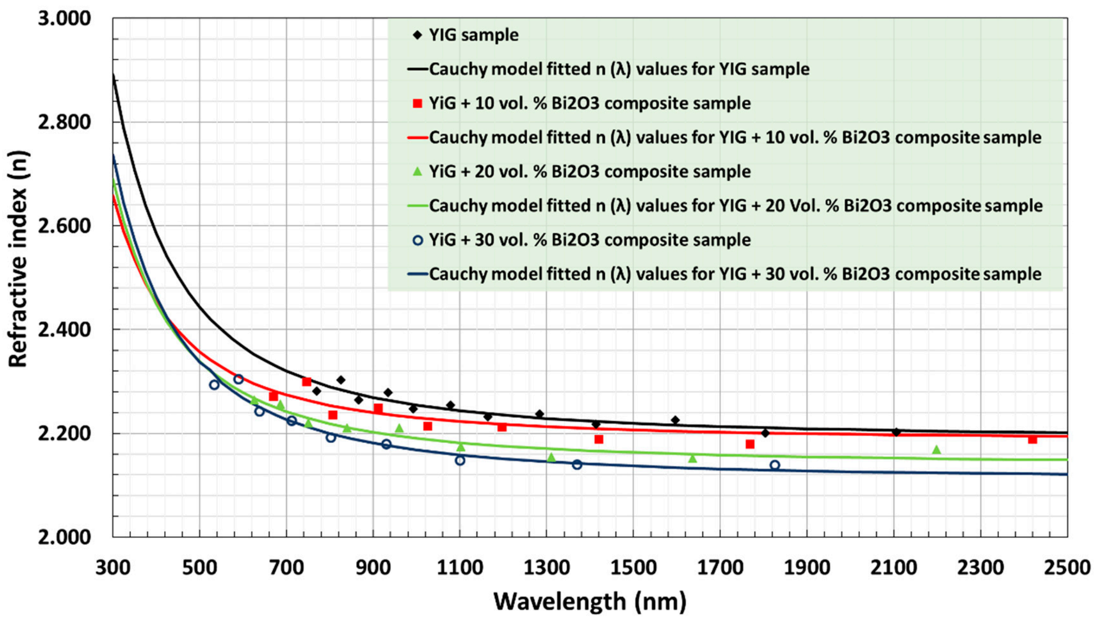

Figure 6. Refractive index dispersion spectra of $Y_3Fe_5O_{12}$ and $Y_3Fe_5O_{12}$: Bi_2O_3 composite thin films. The solid curves were determined according to Cauchy dispersion relationship.

Figure 7 shows the absorption coefficient datasets of YIG and YIG: Bi_2O_3 composite films. These datasets were derived by confirming the film thicknesses using the peak-to-peak fitting of transmission spectra according to the method described in Refs [22-25, 32]. It was found that absorption coefficient is substantially dependent on the added excess Bi_2O_3 content. The higher the bismuth oxide content addition to the nano-composite material system, the lower the absorption coefficients across visible range, which leads to possibilities to engineer these nanomaterial systems according to the required applications.

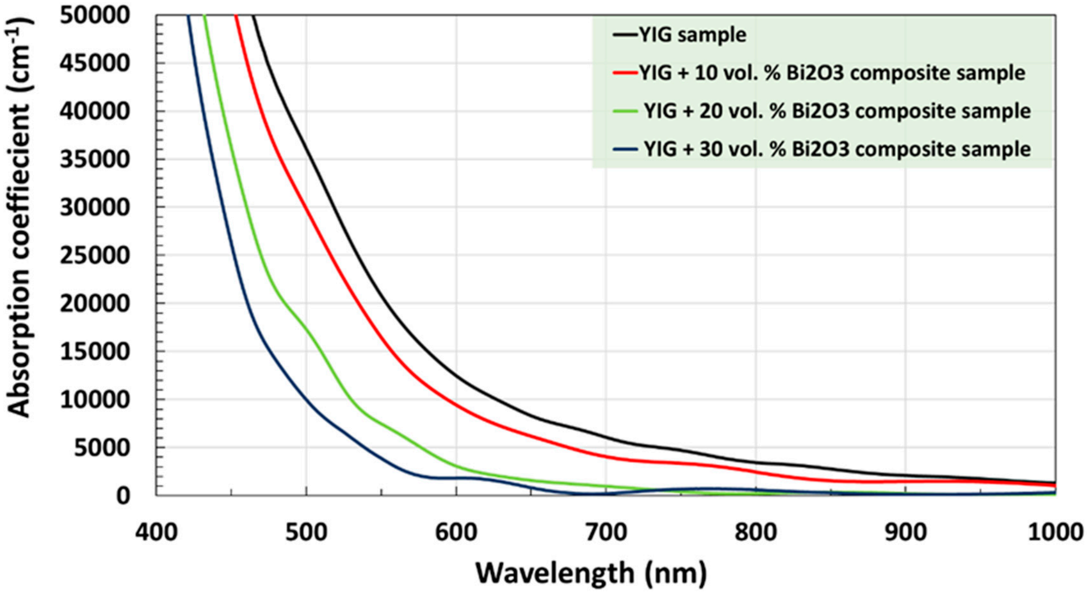

Figure 7. Derived optical absorption coefficient datasets of $Y_3Fe_5O_{12}$ and $Y_3Fe_5O_{12}$: Bi_2O_3 composite samples, obtained with ECU MPC fitting software (across the spectral range 400–1000 nm) by using the measured transmission spectrum data of the samples. The physical film thickness used in fitting was obtained from line slopes (Fig. 4), and the refractive index dispersion function from the Cauchy formula with coefficients obtained from least-squares fitting (Fig. 5).

These optical constants results can add value to the previously published MO dataset properties of similar garnet-type composites, by way of re-confirming the calculations of MO quality factors or the validity of some MPC designs. Overall, the methodologies and results presented can be of interest for the designers of new semitransparent thin-film compositions of all types.

3.2. Optical study of $Bi_3Fe_5O_{12}$ and $Bi_3Fe_5O_{12}$:Dy_2O_3 (11-20 vol. %) composites

Bismuth-substituted metal-doped iron garnets of different composition types having high volumetric fraction of the garnet phase together with giant Faraday rotation and good microstructure quality are very suitable for use as functional materials in applied magneto-optics [10-12, 21-25]. The properties of these types of garnet materials are strongly dependent on the level of bismuth substitution as well as on the synthesis process parameters. The higher the number of bismuth atoms substituted into the garnet system (to replace rare-earth atoms, such as Y, Dy, Lu, or Sm), the greater is the potential to have higher Faraday rotation. So far, garnet films approaching the maximum Bi substitution of three atoms per formula unit, e.g. $Bi_3Fe_5O_{12}$ (BIG) and $Bi_3Fe_4Ga_1O_{12}$, prepared by pulsed laser deposition (PLD) process, demonstrated very large Faraday rotations in the green light [35, 36]. According to our knowledge, there are no reports on RF sputtered films of similar composition type (containing 3 bismuth atoms per formula unit, or deposited from an oxide-mix-based garnet-stoichiometry targets containing more than four iron atoms per f. u. such as $Bi_3Fe_5O_{12}$) that possessed good magneto-optic (MO) performance. However, a co-sputtering process successfully led our group to synthesise a garnet composition stoichiometrically as close as possible to $Bi_3Fe_5O_{12}$, which contained some dysprosium (Dy) dilution. The detailed characteristics of $Bi_3Fe_5O_{12}$: Dy_2O_3 composite films containing different amounts of added dysprosium oxide showing excellent combinations of the optical and magneto-optical properties were reported in Ref [23]. Here, we present the results of the optical constants study of RF sputtered thin films of composition type $Bi_3Fe_5O_{12}$ and $Bi_3Fe_5O_{12}$:Dy_2O_3 (11-20 Vol. %) composite nano-scale layers.

Figure 8 shows the measured transmission spectra of as-deposited $Bi_3Fe_5O_{12}$ garnet and $Bi_3Fe_5O_{12}$:Dy_2O_3 (11-20 vol. %) composite thin film layers. All samples show distinct interference fringes with relatively high wave intensity over a wide range of wavelengths (especially from 600 nm to 2500 nm). It can be noticed that below 600 nm, there is a small number of weak transmission peaks, indicating the higher-wavelength absorption edge, compared to results presented in Section 3.1. A limited number of interference fringes are observed (about five fringes, Fig. 8, curve d) for a composite sample of type $Bi_3Fe_5O_{12}$:Dy_2O_3 (20 vol. %), indicating that the sample was possibly thinner. Our calculated data confirmed that the film thickness for this particular batch of samples was less than 500 nm, as can be seen in Fig. 8d, (slope value 0.858). The detailed calculated values of refractive index at multiple wavelength points and the film thickness data for each sample from these batches are summarised in the Supplementary section (Table S2).

Preprints (www.preprints.org) | NOT PEER-REVIEWED | Posted: 27 February 2019 doi:10.20944/preprints201902.0250.v1

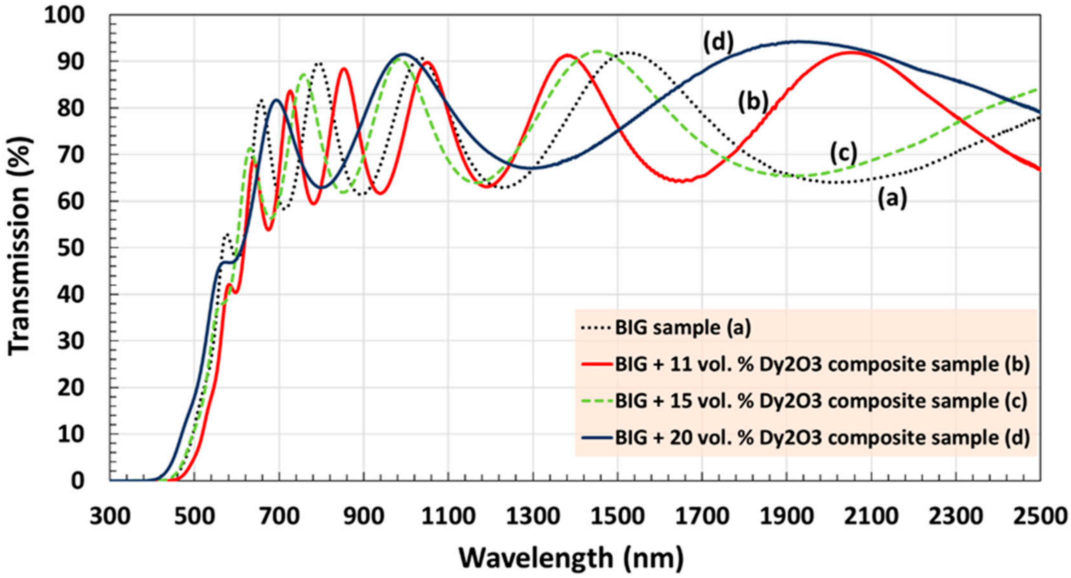

Figure 8. Transmission spectra of $Bi_3Fe_5O_{12}$ and $Bi_3Fe_5O_{12}$:Dy_2O_3 composite thin films.

Figure 9 shows the plots of (l/2) versus (n/λ) for all as-deposited BIG and BIG: Bi_2O_3 composite garnet layers, from which the film thicknesses were recalculated, and then the physical thickness values were found with a relatively small error. The perfectly straight lines of well-defined slopes confirmed the accuracy of the calculated values for each of the samples (as listed in Table S2, in the Supplementary section), and this also validated the modified interference fringes equation (Eq. 3). With the help of the calculated refractive index values (n_2 at each fringe point), from the least-square fitting, the wavelength-dependent refractive index data for each sample were extrapolated across a broad spectral range. Figure 10 shows the least-square fit of the calculated refractive index (n_2) values, and Figure 11 represents the derived refractive index values (from Cauchy model) for the broad spectral range, between 300–2500 nm, for all garnet samples.

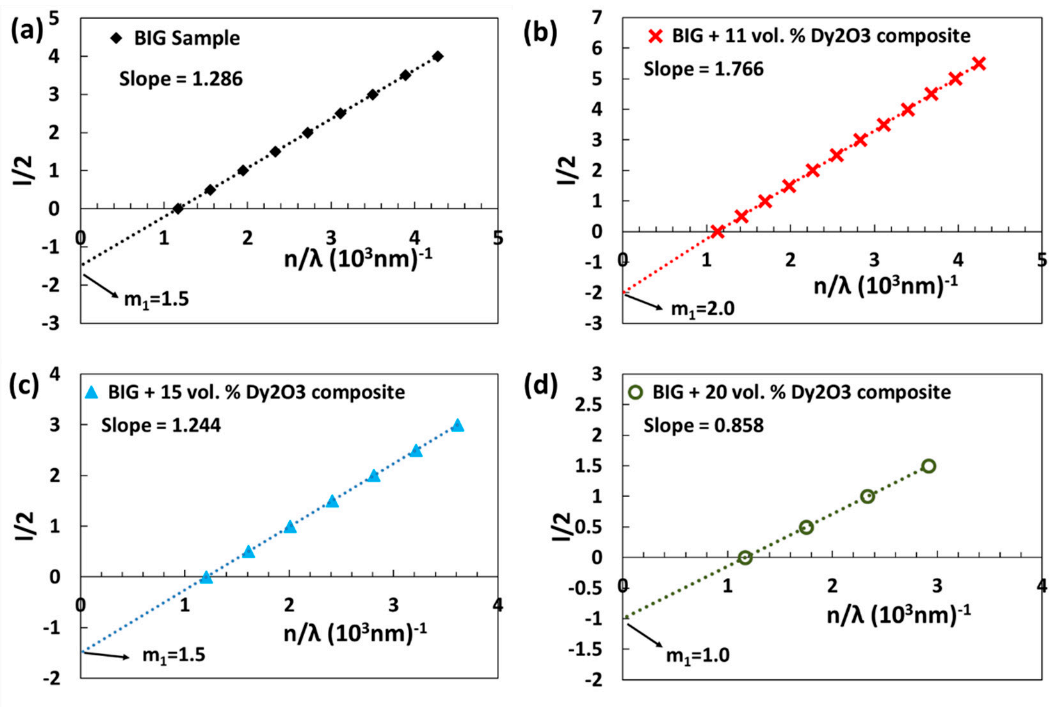

Figure 9. Plots of (l/2) versus (n/λ) used to determine the film thickness and the first-order value m_1 for $Bi_3Fe_5O_{12}$ and $Bi_3Fe_5O_{12}$:Dy_2O_3 composite thin films.

Preprints (www.preprints.org) | NOT PEER-REVIEWED | Posted: 27 February 2019 doi:10.20944/preprints201902.0250.v1

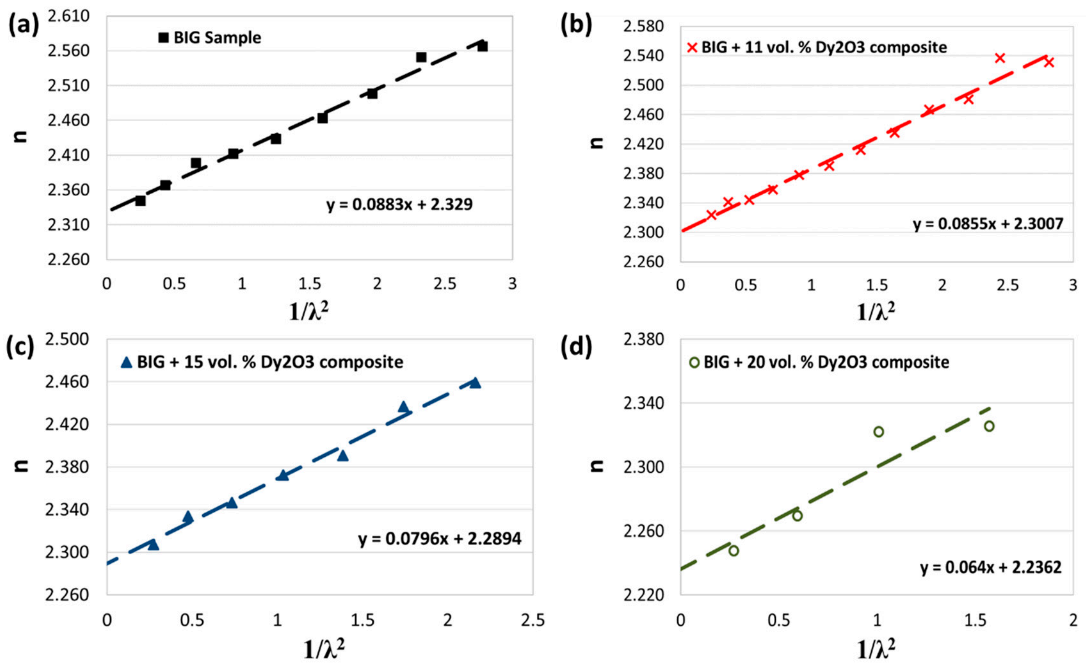

Figure 10. Least-square fit of the calculated refractive index (n_2) values for $Bi_3Fe_5O_{12}$ and $Bi_3Fe_5O_{12}$:Dy_2O_3 composite-type thin films.

It can be seen that the refractive index values gradually decrease noticeably with the increase in the wavelength, up to about 1600 nm, and these remain decreasing with a negligible variance (asymptotically) above that wavelength. The effects of Dy_2O_3 addition to the base material system are quite clear. The refractive index values decreased as the number of excess metal-oxide content increased in the film layer volumes. All of the composite samples exhibited a much lower refractive index values, compared to these of pure BIG sample, which indicated that the dysprosium oxide diluted the oxide mix sputtered from the $Bi_3Fe_5O_{12}$ target. This could be expected to lead, after running the annealing crystallization process, to forming an incompletely-substituted dysprosyum iron garnet composition, volume-diluted by extra dysprosium oxide in a solid-solution-type phase. We know from experiments that many metal oxides (including Dy_2O_3) dissociate during sputtering deposition in pure-argon plasma, since the as-deposited metal oxide layers often require a high-temperature annealing process to regain their expected optically-clear appearance. The absorption coefficient values for all samples deposited were also found to be quite promising (as shown in Fig. 12).

Preprints (www.preprints.org) | NOT PEER-REVIEWED | Posted: 27 February 2019 doi:10.20944/preprints201902.0250.v1

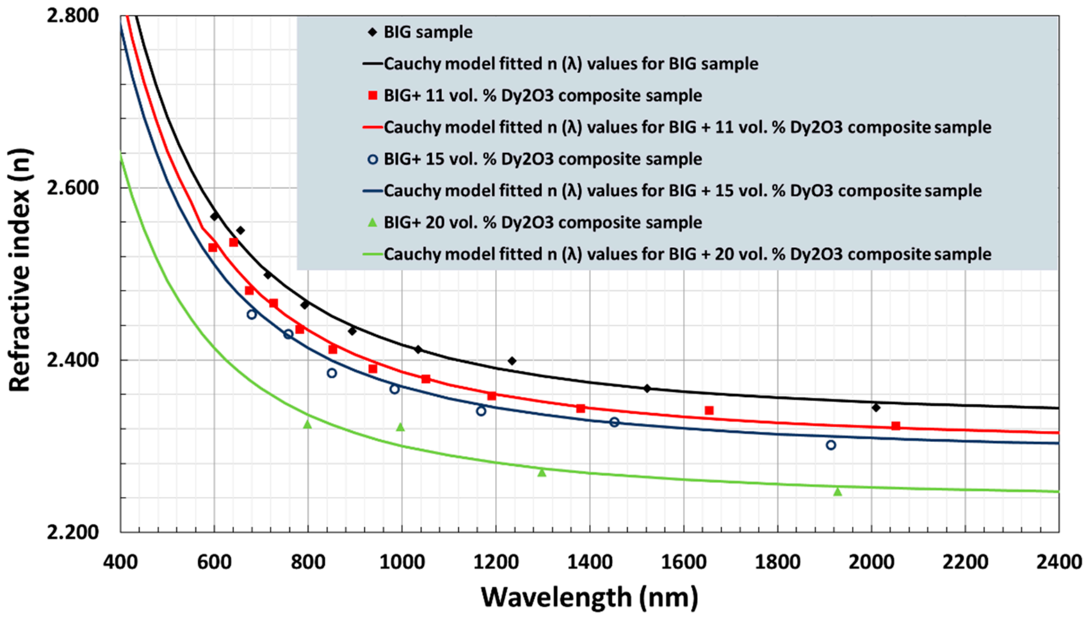

Figure 11. Refractive index dispersion spectra for $Bi_3Fe_5O_{12}$ and $Bi_3Fe_5O_{12}$:Dy_2O_3 composite thin films. The solid curves were determined according to Cauchy dispersion relationship and the marked data points represent the calculated n_2 values for each of the samples.

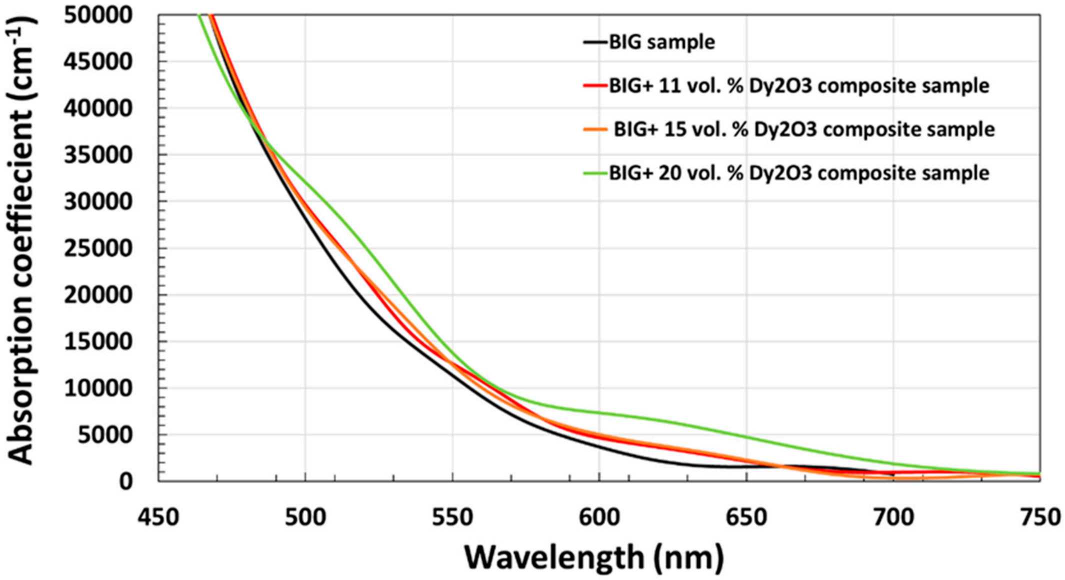

Figure 12. Derived absorption coefficient datasets for $Bi_3Fe_5O_{12}$ and $Bi_3Fe_5O_{12}$:Dy_2O_3 composite samples.

The MPC software-based fitting procedure derived the absorption coefficients almost across the entire visible range for all garnet samples, and these data are plotted in Fig. 12. The effects of Dy_xO_y dilution are also noticeable, manifesting as rather small changes in the nanocomposite absorption spectra. The higher the oxide dilution, the higher was the absorption coefficient in the as-deposited samples. It can be expected that in crystallized (annealed) garnet-type samples, an opposite trend will be observed: the more Bi atoms in dodecahedral sites replaced by Dy, the small absorption coefficients.

Preprints (www.preprints.org) | NOT PEER-REVIEWED | Posted: 27 February 2019 doi:10.20944/preprints201902.0250.v1

3.3. Optical study of $Bi_{1.8}Lu_{1.2}Fe_{3.9}Al_{1.1}O_{12}$ and $Bi_{1.8}Lu_{1.2}Fe_{3.9}Al_{1.1}O_{12}$:$Bi_2O_3$ (5-20 vol. %) composites

Highly Bi-substituted lutetium iron garnet thin films of composition type $(BiLu)_3(FeAl)_5O_{12}$ are a wonderful subclass of MO garnet materials that features strong in-plane magnetization component with magnetically-soft switching behaviour suitable for various magneto-optical applications in nonreciprocal integrated optics, magneto-photonic crystals and waveguides, as well as magnetic field imaging and sensing devices. Liquid-phase epitaxy (LPE) grown monocrystalline films of a similar composition type $(BiLu)_3(FeAl)_5O_{12}$ possessed in-plane magnetic anisotropy suitable for magnetic flux visualization in high-T_c superconductors [37]. However, LPE technique has some limitations in terms of achieving high bismuth substitution levels in the films. RF magnetron sputtering is one of the ideal alternatives to produce high-quality, highly Bi-substituted iron garnet films. A garnet material with a composition type $Bi_{1.8}Lu_{1.2}Fe_{3.9}Al_{1.1}O_{12}$ (BiLuIG) is expected to have a lattice parameter of 12.384 Å, very close to that of gadolinium gallium garnet (GGG) substrates (12.383 Å), imperative for the high-quality material growth as well as for the development of practical on-chip MO devices. Previously, we have reported on the optimization of sputter-deposition process parameters and the characterization of MO properties in garnet layers of composition type $Bi_{1.8}Lu_{1.2}Fe_{3.9}Al_{1.1}O_{12}$. We have also experimentally confirmed that the co-sputtering approach ($Bi_{1.8}Lu_{1.2}Fe_{3.9}Al_{1.1}O_{12}$:$Bi_2O_3$) improved the MO quality of these types of garnet materials and allowed to adjust the lattice parameter values as well [24]. This subsection is intended to provide the experimentally obtained results of the optical constants study of RF sputtered thin film garnet layers of composition type $Bi_{1.8}Lu_{1.2}Fe_{3.9}Al_{1.1}O_{12}$ and also $Bi_{1.8}Lu_{1.2}Fe_{3.9}Al_{1.1}O_{12}$:$Bi_2O_3$ (5-20 Vol. %) composites.

Thickness-dependent number of interference fringes has been observed in the transmission spectra of BiLuIG and BiLuIG: Bi_2O_3 garnet composite layers. Figure 13 shows the plots of transmission spectra of thin garnet layers on glass, for a wide spectral range of 300-2500 nm. The high amplitude transmission fringes confirmed the achievement of both the good optical homogeneity, substrate interface quality, and the excellent film surface quality. It can be noticed that all samples exhibited multiple transmission fringes with large amplitude with high optical transparency. In the long-wavelength region (especially after 1100 nm), the fringes are found to be much wider spectrally, compared to those in the short-wavelength region (about 500-1100 nm). The reason is "normal" refractive index dispersion function (lower index in the long-wavelength range). The very sharp fundamental absorption edge values are observed in between 400-500 nm. The addition of Bi_2O_3 content pushes the absorption edge towards the shorter wavelength, as can be seen in Fig. 13. The results of the optical constants study for these material types are summarized in Table S3 (in the Supplementary section), followed by tabulating the transmission maxima (T_M) and minima (T_m) values from the obtained transmission spectra.

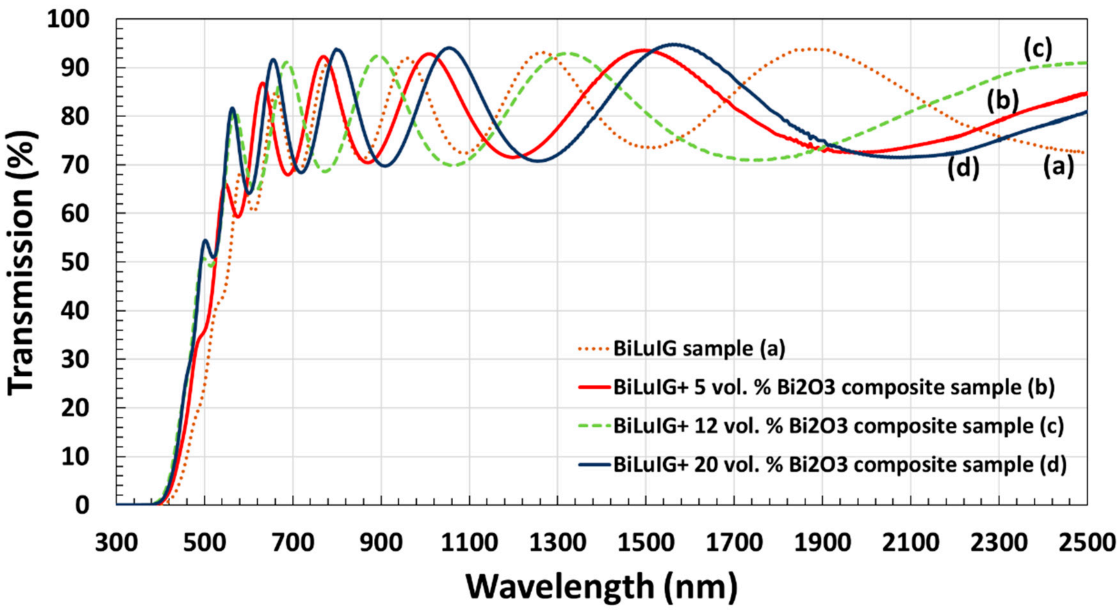

Figure 13. Transmission spectra of $Bi_{1.8}Lu_{1.2}Fe_{3.9}Al_{1.1}O_{12}$ and $Bi_{1.8}Lu_{1.2}Fe_{3.9}Al_{1.1}O_{12}$:$Bi_2O_3$ composite thin films.

Preprints (www.preprints.org) | NOT PEER-REVIEWED | Posted: 27 February 2019 doi:10.20944/preprints201902.0250.v1

Figure 14 illustrates the plots of (l/2) versus (n/λ) for all as-deposited BiLuIG and BiLuIG: Bi_2O_3 composite garnet layers, which were found to form straight lines, indicating that relatively high-accuracy film thickness values were obtained. From these simple and appealing graphical presentations, the values of film thicknesses and correct interference order numbers for each sample were calculated, as listed in Table S3, in the Supplementary section. On the other hand, Figure 15 shows the least-square fit of the calculated refractive index (n_2) values, which helped determine the broad-range spectrally-dependent refractive index Cauchy's dispersion model parameters.

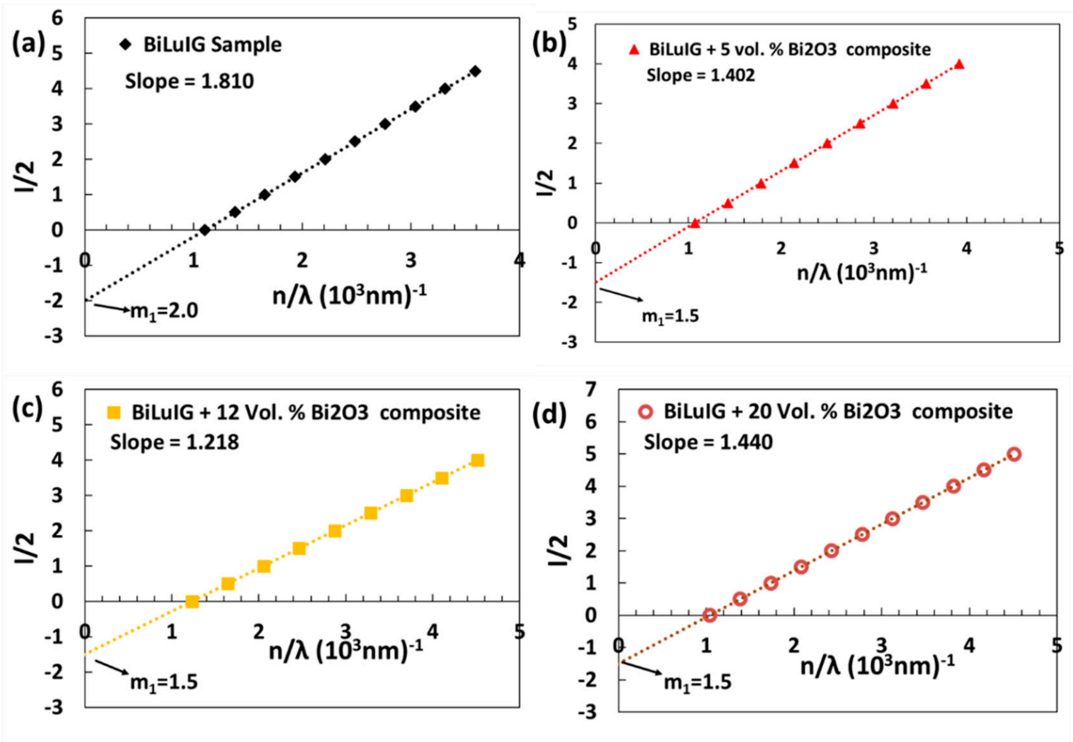

Figure 14. Plots of (l/2) versus (n/λ) used to determine the film thickness and the first-order values m_1 for $Bi_{1.8}Lu_{1.2}Fe_{3.9}Al_{1.1}O_{12}$ and $Bi_{1.8}Lu_{1.2}Fe_{3.9}Al_{1.1}O_{12}$:$Bi_2O_3$ composite thin films.

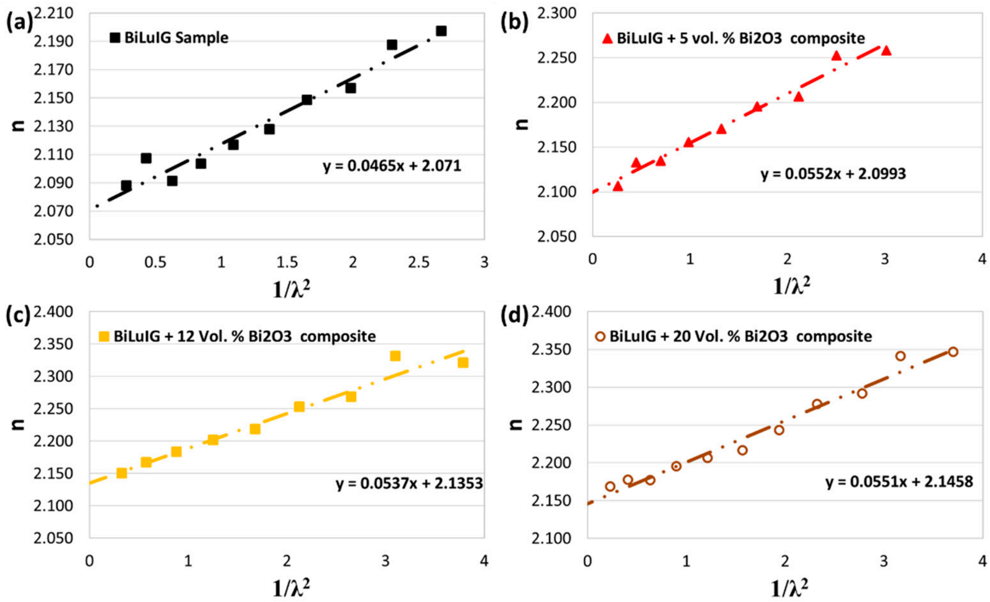

Figure 15. Least-square fit of the calculated refractive index (n_2) values for $Bi_{1.8}Lu_{1.2}Fe_{3.9}Al_{1.1}O_{12}$ and $Bi_{1.8}Lu_{1.2}Fe_{3.9}Al_{1.1}O_{12}$:$Bi_2O_3$ composite thin films.

Preprints (www.preprints.org) | NOT PEER-REVIEWED | Posted: 27 February 2019 doi:10.20944/preprints201902.0250.v1

The calculated refractive indices at different wavelengths derived from Cauchy's relation as well as the calculated refractive index data points (n_2 values obtained using T_M and T_m) are plotted in Fig. 16. It can be noted that the refractive index (n) is in the range of 2.1-2.5 in the visible region and decreases with increasing wavelength, up to a certain extent. In the long-wavelength region (above 1600 nm), the refractive index seems to be asymptotically approaching a constant value. The volumetric fraction of Bi_2O_3 introduced into the BiLuIG system helps increase the refractive index of the composite films, however, it shifts the absorption edge towards the shorter wavelength region (as seen in Fig. 13). This is expected, in both the as-deposited and also in crystallized samples with high Bi substitution. It can be seen that much lower absorption coefficient has been observed in composite films compared to that of $Bi_{1.8}Lu_{1.2}Fe_{3.9}Al_{1.1}O_{12}$ garnet layer as shown in Fig. 17.

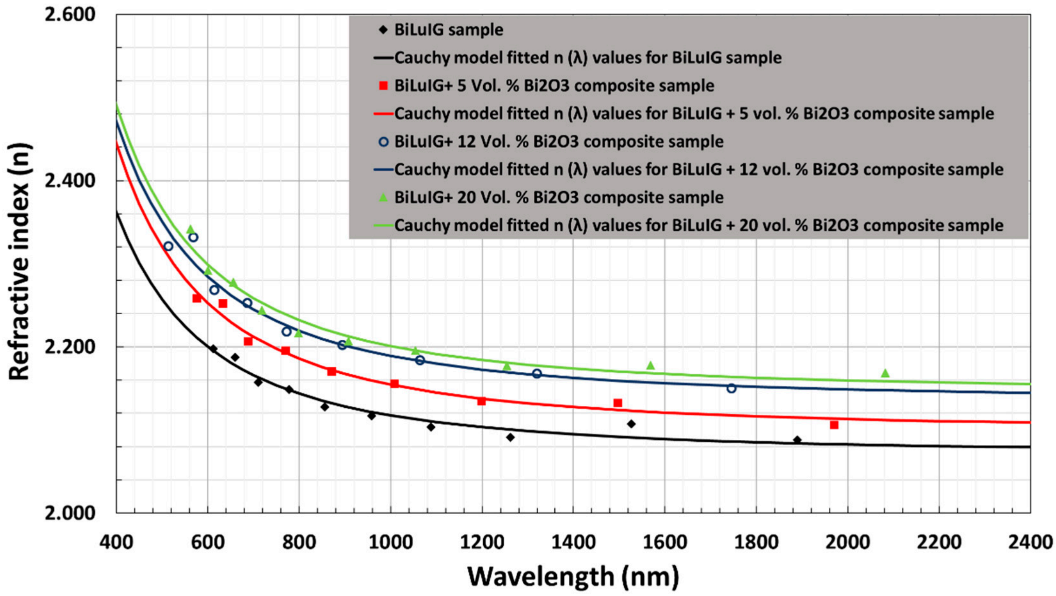

Figure 16. Refractive index dispersion spectra for $Bi_{1.8}Lu_{1.2}Fe_{3.9}Al_{1.1}O_{12}$ and $Bi_{1.8}Lu_{1.2}Fe_{3.9}Al_{1.1}O_{12}$:$Bi_2O_3$ composite thin films. The solid curves were determined according to Cauchy dispersion relationship.

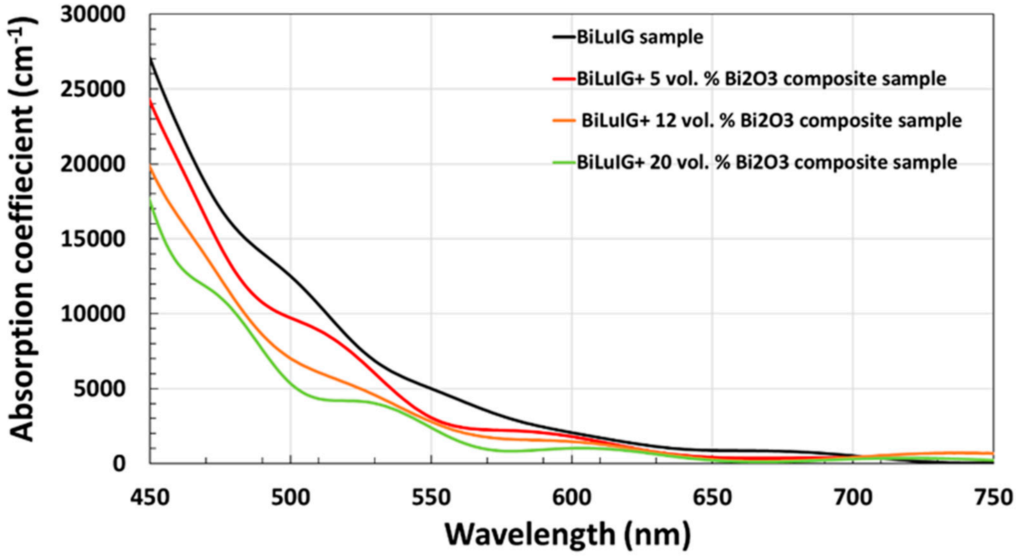

Figure 17. Derived absorption coefficient and extinction coefficient datasets for the as-deposited $Bi_{1.8}Lu_{1.2}Fe_{3.9}Al_{1.1}O_{12}$ and $Bi_{1.8}Lu_{1.2}Fe_{3.9}Al_{1.1}O_{12}$:$Bi_2O_3$ composite samples.

 doi:10.20944/preprints201902.0250.v1

Figure 17 represents the plots of absorption coefficient across most of the visible range for all samples, where the effects of Bi_2O_3 addition can be noticed. The absorption coefficient values decrease with the increasing excess bismuth-oxide content, as expected. Since the as-deposited nanocomposite-type layers are composed of a solid-solution-type mix of several oxides (some of which are metal-rich due to sputtering-induced oxygen loss), the wave-like variations in the spectra are observed (these are not a fitting process artefact). After running composition-optimized annealing crystallization processes, the bulk of film layers will be dominated by garnet phase, partially diluted by the excess oxide. In these layers, strong Faraday rotation is observed, and the "waves" in the fitted absorption coefficient spectra disappear [24].

4. Conclusions

We have successfully evaluated the optical constants (spectral dependencies of the refractive index for wavelengths between 400 nm to over 2000 nm) for several rare-earth substituted ferrite-type iron garnets and garnet-oxide nanocomposites by using only the transmission spectra datasets. The methodologies used for the derivation of these optical constants datasets have been described. Whilst the datasets have been evaluated in amorphous-phase (as-deposited) RF sputtered films only, a wide range of garnet compositions containing different rare-earth substituting ions have been characterised.

Supplementary Materials: The datasets summarized in tables (S1, S2 and S3) are also provided.

Author Contributions: M.N.-E.A. performed the experiments and analyzed the data; M.N.-E.A. and M.V. discussed the data and prepared the manuscript; K.A. reviewed and improved the manuscript.

Funding: Electron Science Research Institute, Edith Cowan University, Australia.

Conflicts of Interest: The authors declare no conflict of interest.

References

1. Zvezdin, A.K.; Kotov, V.A. Modern Magnetooptics and Magnetooptical Materials; Institute of Physics Publishing: Bristol, UK, 1997.
2. Eppler, W. R.; Kryder, M. H. Garnets for short wavelength magneto-optic recording. J. Phys. Chem. Solid. 1995, 56 (11), 1479-1490.
3. Aichele, T.; Lorenz, A.; Hergt, R.; Gornert, P. Garnet layers prepared by liquid phase epitaxy for microwave and magneto-optical applications—A review. Cryst. Res. Technol. 2003, 38, 575–578.
4. Scott, G.B.; Lacklison, D.E. Magnetooptic properties and applications of Bismuth substituted iron garnets. IEEE Trans. Magn. 1976, 12, 292–311.
5. Zhou, B.; Zhang, Y. W.; Liao, C. S.; Yan, C. H.; Chen, L. Y.; Wang, S. Y. Rare-earth-mediated magnetism and magneto-optical kerr effects in nanocrystalline CoFeMn0.9Re0.1O4 thin films. J. Mag. Mag. Mat. 2004, 280, 327-333.
6. Goto, T.; Onbasli, M. C.; Ross, C. A. Magneto-optical properties of cerium substituted yttrium iron garnet films with reduced thermal budget for monolithic photonic integrated circuits. Optics Express. 2012, 20 (27), 28507-28517.
7. Walker, L. Ferromagnetic resonance in Terbium-doped Yttrium iron garnet. J. Appl. Phys. 1962, 33, 1243–1247.
8. Xu, H.; Yang, H. Magnetic properties of YIG doped with cerium and gadolinium ions. J. Mater. Sci. Mater. Electron. 2008, 19, 589–593.

Preprints (www.preprints.org) | NOT PEER-REVIEWED | Posted: 27 February 2019 doi:10.20944/preprints201902.0250.v1

9. Elhamali, S.M.; Ibrahim, N.B.; Radiman, S. Structural, optical and magnetic properties of YIG doped with Erbium and Terbium nanofilms using sol-gel method. J. Adv. Nanomater. 2016, 1, 11–20.
10. Challeton, D.; Bechevet, B.; Rolland, B.; Armand, M.F. RF sputtered Bi-substituted garnet film for magneto-optic memory. J. Magn. Magn. Mater. 1990, 83, 37–38.
11. Kim, Y.H.; Kim, J.S.; Kim, S.I.; Levy, M. Epitaxial growth and properties of Bi-substituted Yttrium-Iron-garnet film grown on (111) Gadolinium-Gallium-garnet substrates by rf magnetron sputtering. J. Korean Phys. Soc. 2003, 43, 400–405.
12. Sekhar, R.K.; Singh, M.R. Fabrication and characterization of Bismuth-Cerium composite iron garnet epitaxial films for magneto optical applications. J. Appl. Phys. 2012, 112, 083525.
13. Kim, H.; Grishin, A.M.; Rao, K.V. Giant Faraday rotation of blue light in epitaxial CexY3−xFe5O12 films grown by pulsed laser deposition. J. Appl. Phys. 2001, 89, 4380–4383.
14. Nistor, I.; Holthaus, C.; Mayergoyz, I.D.; Krafft, C. Development of liquid phase epitaxy-grown (Bi, Gd, Lu) substituted thin-film iron garnets. J. Appl. Phys. 2006, 99, 08M702.
15. Shoji, Y.; Mizumoto, T. Silicon waveguide optical isolator with directly bonded magneto-optical garnet. Apl. Sci. 2019, 9, 609.
16. Du, Q.; Fakhrul, T.; Zhang, Y.; Hu, J.; Ross, C. A. Monolithic magneto-optical oxide thin films for on-chip optical isolation. MRS Bulletin. 2018, 43, 413-418.
17. Bi, l.; Hu, J.; Jiang, P.; Kim, H. S.; Kim, D. H.; Onbasli, M. C.; Dionne, F. F.; Ross, C. A. Magneto-optical thin films for on-chip monolithic integration of non-reciprocal photonic devices. Materials. 2013, 6, 5094-5117.
18. Drezdzon, S. M.; Yoshie, T. On-chip waveguide isolator based on bismuth iron garnet operating via nonreciprocal single-mode cutoff. Opt. Express. 2009, 17 (11) 9276-9281.
19. Levy, M. The on-chip integration of magnetooptic waveguide isolators. IEEE, Quantum elec. 2002, 8(6), 1300-1306.
20. Stupakiewicz, A.; Szerenos, K.; Davydova, M. D.; Zvezdin, K. A.; Zvezdin, A. K.; Kirilyuk, A.; Kimel, A. V. Selection rules for all-optical magnetic recording in iron magnet. Nat. Communications. 2019, doi.org/10.1038/s41467-019-08458-w.
21. Nur-E-Alam, M.; Vasiliev, M.; Kotov, V.A.; Alameh, K. Recent developments in magneto-optic garnet-type thin-film materials synthesis. Procedia Eng. 2014, 76, 61–73.
22. Vasiliev, M.; Alam, M.N.; Kotov, V.A.; Alameh, K.; Belotelov, V.I.; Burkov, V.I.; Zvezdin, A.K. RF magnetron sputtered (BiDy)3(FeGa)5O12:Bi2O3 composite garnet-oxide materials possessing record magneto-optic quality in the visible spectral region. Opt. Express 2009, 17, 19519–19535.
23. Alam, M.N.; Vasiliev, M.; Alameh, K. Bi3Fe5O12:Dy2O3 composite thin film materials for magneto-photonics and magneto-plasmonics. Opt. Mater. Express 2014, 4, 1866–1875.
24. Alam, M.N.; Vasiliev, M.; Kotov, V.A.; Alameh, K. Highly bismuth-substituted, record-performance magneto-optic garnet materials with low coercivity for applications in integrated optics, photonic crystals, imaging and sensing. Opt. Mater. Express 2011, 1, 413–427.
25. Alam, M.N.; Vasiliev, M.; Alameh, K.; Kotov, V.A.; Demidov, V.; Balabanov, D. YIG:Bi2O3 Nanocomposite thin films for magnetooptic and microwave applications. J. Nanomater. 2015, 182691, doi:10.1155/2015/182691.
26. Manifacier, J.C.; Gasiot, J.; Fillard, J.P. A simple method for the determination of the optical constants n, k and the thickness of a weakly absorbing thin film. J. Phys. E Sci. Instrum. 1976, 9, 1002–1004.
27. Swanepoel, R. Determination of the thickness and optical constants of amorphous silicon. J. Phys. E Sci. Instrum. 1983, 16, 1214–1222.
28. Hassanien, A.S.; Aly, K.A.; Akl, A.A. Study of optical properties of thermally evaporated ZnSe thin films annealed at different pulsed laser powers. J. Alloys Compd. 2016, 685, 733–742.

 doi:10.20944/preprints201902.0250.v1

29. Nenkov, M. R.; Pencheva, T. G. Determination of thin film refractive index and thickness by means of film phase thickness, Cent. Eur. J. Phys. 2008, 6(2), 332-343.
30. Aly, K.A. Optical band gap and refractive index dispersion parameters of AsxSe70Te30−x (0 ≤ x ≤ 30 at. %) amorphous films. Appl. Phys. A 2010, 99, 913, doi:10.1007/s00339-010-5680-6.
31. Dahshan, A.; Amer, H.H.; Aly, K.A. Compositional dependence of the optical constants of amorphous GexAs20Se80−x thin films. J. Phys. D Appl. Phys. 2008, 41, 215401.
32. Alam, M.N.; Vasiliev, M.; Alameh, K. Properties of ferrite garnet (Bi, Lu, Y)3(Fe, Ga)5O12 thin film materials prepared by RF magnetron sputtering. Nanomaterials. 2018, 8, 355.
33. Alam, M.N.; Vasiliev, M.; Alameh, K. High-performance RF-sputtered Bi-substituted iron garnet thin films with almost in-plane magnetization. Opt. Mat. Express. 2017, 7 (3), 676-686.
34. Emam-Ismail, M.; El-Hagary, M.; Shaaban, E.R.; Al-Hedeib, A.M. Microstructure and optical studies of electron beam evaporated ZnSe1−xTex nanocrystalline thin films. J. Alloys Compd. 2012, 532, 16–24.
35. Deb, M.; Popova, E.; Fouchet, A.; Keller, N. Magneto-optical Faraday spectroscopy of completely bismuth-substituted Bi3Fe5O12 garnet thin films. J. Phys. D Appl. Phys. 2012, 45(45), 455001.
36. Kang, S.; Yin, S.; Adyam, V.; Li, Q.; Zhu, Y. Bi3Fe4Ga1O12 garnet properties and its application to ultrafast switching in the visible spectrum. IEEE Trans. Magn. 2007, 43, 3656–3660.
37. Adachi, N.; Obata, K.; Okuda, T.; Machi, T.; Koshizuka, N. Synthesis of Bi-Lu-substituted Iron Garnet Films for Visualization of Magnetic Flux in High-Tc Superconductors. Jpn. J. Appl. Phys. 2002, 41 (Part1, 10), 5986–5990.